

## INITIAL-FINAL MASS RELATION FOR 3 TO 4 $M_{\odot}$ PROGENITORS OF WHITE DWARFS FROM THE SINGLE CLUSTER NGC 2099<sup>1</sup>

JEFFREY D. CUMMINGS<sup>2</sup>, JASON S. KALIRAI<sup>3,2</sup>, P.-E. TREMBLAY<sup>3,5</sup>, AND ENRICO RAMIREZ-RUIZ<sup>4</sup>

*Draft version October 11, 2018*

### ABSTRACT

We have expanded the sample of observed white dwarfs in the rich open cluster NGC 2099 (M37) with the Keck Low-Resolution Imaging Spectrometer. Of 20 white dwarf candidates, the spectroscopy shows 19 to be true white dwarfs with 14 of these having high S/N. We find 11 of these 14 to be consistent with singly evolved cluster members. They span a mass range of  $\sim 0.7$  to  $0.95 M_{\odot}$ , excluding a low-mass outlier, corresponding to progenitor masses of  $\sim 3$  to  $4 M_{\odot}$ . This region of the initial final mass relation (IFMR) has large scatter and a slope that remains to be precisely determined. With this large sample of white dwarfs that belong to a single age and metallicity population, we find an initial-final mass relation of  $(0.171 \pm 0.057)M_{\text{initial}} + 0.219 \pm 0.187 M_{\odot}$ , significantly steeper than the linear relation adopted over the full observed white dwarf mass range in many previous studies. Comparison of this new relation from the solar metallicity NGC 2099 to 18 white dwarfs in the metal-rich Hyades and Praesepe shows that their IFMR also has a consistently steep slope. This strong consistency also suggests that there is no significant metallicity dependence of the IFMR at this mass and metallicity range. As a result, the IFMR can be more reliably determined with this broad sample of 29 total white dwarfs giving  $M_{\text{final}} = (0.163 \pm 0.022)M_{\text{initial}} + 0.238 \pm 0.071 M_{\odot}$  from  $M_{\text{initial}}$  of 3 to  $4 M_{\odot}$ . A steep IFMR in this mass range indicates that the full IFMR is nonlinear.

### 1. INTRODUCTION

White dwarfs are by far the most common end point of stellar evolution and are a valuable tool for understanding a variety of processes at both the stellar and galactic scales. A key aspect in stellar evolution research is the initial final mass relation (IFMR), where white dwarf masses are compared directly to the zero-age main sequence (ZAMS) mass of their progenitors. This provides a direct measurement of the integrated mass loss that occurs during a stellar lifetime and its dependence on stellar mass. The IFMR gives critical input for a variety of topics, including stellar feedback in galaxy models (Agertz & Kravtsov 2014), interpreting the white dwarf luminosity function (Catalán et al. 2008), providing a way to measure the age of the Galactic halo (Kalirai 2013), and predicting Type Ia supernovae rates (Pritchett et al. 2008; Greggio 2010).

Weidemann (1977) was the first to analyze the IFMR by comparing mass-loss models (Fusi-Peccì & Renzini 1976) to the observed spectroscopic masses of a few white dwarfs in the nearby Hyades and Pleiades clusters. He concluded that the models greatly underestimated the observed mass loss. Subsequent spectroscopic observations of white dwarfs in nearby open clusters provided

further constraints on the IFMR (Koester & Reimers 1981, 1985, 1993, 1996; Reimers & Koester 1982, 1989, 1994; Weidemann & Koester 1983; Weidemann 1987; Jeffries 1997). These studies resulted in a broad but sparsely populated relation (see Weidemann 2000 for review) that shows a clear trend with higher mass main-sequence stars producing increasingly more massive white dwarfs.

More recently, the amount of data constraining the IFMR has greatly increased (e.g., Claver et al. 2001; Dobbie et al. 2004, 2006; Williams et al. 2004; Kalirai et al. 2005; Liebert et al. 2005; Williams & Bolte 2007; Kalirai et al. 2007; Kalirai et al. 2008; Rubin et al. 2008; Kalirai et al. 2009; Williams et al. 2009; Dobbie & Baxter 2010; Dobbie et al. 2012). While these newer data still retain the general trend observed in the earlier IFMR, the scatter in the relation is significant. Is this scatter indicative of stochastic mass loss for stars at the same initial mass, or dependencies on metallicity or environmental effects, or is this scatter simply the result of systematic differences between these studies? One likely contributing systematic is the challenge in defining the ages of the clusters these white dwarfs belong to, which creates uncertainty in the calculated lifetimes of their progenitor stars. This is not only due to uncertainty in the isochrone fitting to photometry itself, in particular for clusters with poorly defined turnoffs and red giant clumps and branches, but that different studies commonly adopt different model isochrones. Additionally, as discussed in Salaris et al. (2009), for many studies the input physics for the adopted isochrones differ from that of the evolutionary models adopted to calculate the white dwarf progenitor masses. All of these factors systematically affect the adopted initial masses of the white dwarfs and can introduce large systematic differences between white dwarfs from different clusters and those analyzed by different groups.

<sup>1</sup> Based on observations with the W.M. Keck Observatory, which is operated as a scientific partnership among the California Institute of Technology, the University of California, and NASA, was made possible by the generous financial support of the W.M. Keck Foundation.

<sup>2</sup> Center for Astrophysical Sciences, Johns Hopkins University, Baltimore, MD 21218, USA; jcummi19@jhu.edu

<sup>3</sup> Space Telescope Science Institute, 3700 San Martin Drive, Baltimore, MD 21218, USA; jkalirai@stsci.edu, tremblay@stsci.edu

<sup>4</sup> Department of Astronomy and Astrophysics, University of California, Santa Cruz, CA 95064; enrico@ucolick.org

<sup>5</sup> Hubble Fellow

Variations in cluster metallicity may also play a role in the scatter associated with the IFMR. The effect of metallicity on the IFMR has been modeled by Marigo & Girardi (2007) and Meng et al. (2008), and they both predict that at the same progenitor masses even moderately metal-poor stars ( $[\text{Fe}/\text{H}] \sim -0.3$ ) result in more massive white dwarfs (by  $\sim 0.05 M_{\odot}$ ) in comparison solar metallicity. Observationally, evidence for the IFMR's metallicity dependence has been found in the extremely metal-rich cluster NGC 6791 ( $[\text{Fe}/\text{H}] = +0.47 \pm 0.04$ ; Gratton et al. 2006), where the observed lower-mass white dwarfs appear to be undermassive relative to the field distribution (Kalirai et al. 2007). In contrast to this, we note that for the moderate-mass white dwarfs that we focus on in our study, both models predict that the IFMR for moderately metal-rich stars ( $[\text{Fe}/\text{H}] \sim 0.15$ ) is not meaningfully different from the solar metallicity IFMR, with final masses different by less than  $0.01 M_{\odot}$ .

First, to limit these effects of varying metallicity and open cluster age uncertainty, we can analyze a large sample of white dwarfs from a single open cluster that is rich with a well defined turnoff and red giant clump, giving a detailed isochrone fit. The intermediate aged ( $520 \pm 50$  Myr; Kalirai et al 2001; hereafter K01) open cluster NGC 2099 (M37) is an ideal cluster for this. The white dwarfs presented here from NGC 2099 cover masses from 0.7 to  $0.95 M_{\odot}$ , a region of the IFMR that still exhibits large scatter and an uncertain slope. Second, with a concern for robustness, we have compared our results to the similar mass range of 18 white dwarfs observed in the Hyades and Praesepe. Because these three clusters span a moderate range of metallicity, this also directly tests the metallicity dependence of the IFMR in this mass and metallicity range ( $0.0 \lesssim [\text{Fe}/\text{H}] \lesssim 0.15$ ). Both the Hyades and Praesepe provide a valuable reference for our work because their age and metallicities are well determined and their white dwarfs are bright with high signal to noise (S/N) spectroscopy; we take their parameters from the consistent analysis performed by Kalirai et al. (2014).

The structure of this paper is as follows, in Section 2 we discuss both the photometric and spectroscopic observations that provide the foundation for this work. In Section 3 we discuss our white dwarf spectroscopic analysis. In Section 4 we discuss our cluster membership determinations. In Section 5 we discuss the NGC 2099 IFMR and compare to that of the Hyades and Praesepe. In Section 5 we discuss our conclusions. Lastly, the Appendix includes a discussion of the last 20 years of cluster parameters analysis for NGC 2099 and justification for our adopted values.

## 2. OBSERVATIONS

Based on the deep photometric observations of NGC 2099 with the Canada-France-Hawaii telescope (K01), a sample of 67 white dwarf candidates were found in the central  $15'$  in NGC 2099. From comparison to a nearby off-cluster field, approximately 50 of these white dwarf candidates were estimated to be cluster white dwarfs. Observations of white dwarf candidates have been performed with Keck I using the Low Resolution Imaging Spectrometer (LRIS; Oke et al. 1995) and with Gemini using GMOS. With Keck I, 22 white dwarf candidate spectra were acquired across two  $5' \times 7'$  fields using two multi-object spectrum masks (F1 and F2). For spec-

tral flux calibration, flux standards were observed each night using long-slit spectral observations at the same settings. During the first observations on 2002 December 4, the F1 and F2 masks were each observed for 6000 seconds using the 600/4000 grism, giving a resolution of  $\sim 4 \text{ \AA}$  and a dispersion of  $\sim 0.6 \text{ \AA}$  per pixel, (Program ID: U45L-2002B; PI: B. Hansen, UCLA).<sup>6</sup> During the second observations on 2008 December 23 and 24, the F2 mask only was observed for 9600 seconds the first night and 13200 seconds the second night. These 2008 observations used the slightly lower resolution 400/3400 grism, giving a resolution of  $\sim 6 \text{ \AA}$  and a dispersion of  $\sim 1.1 \text{ \AA}$  per pixel, (Program ID: U077LA-2008B; PI: E. Ramirez-Ruiz, UCSC). Both grisms give spectra that span a series of five Balmer lines ( $\text{H}\beta$ ,  $\text{H}\delta$ ,  $\text{H}\gamma$ ,  $\text{H}\epsilon$ , and  $\text{H}8$ ) that are sensitive to stellar temperature and surface gravity. The observing conditions were clear with subarcsecond seeing during 2002 December 4. The conditions were similarly good during 2008 December 23 but relatively poor during 2008 December 24.

Unlike the F1 mask, which was observed only in 2002, the F2 mask was observed twice with two different grisms. The 2008 F2 observations were significantly deeper than the 2002 F2 observations, so we have focused on the 2008 data and do not attempt to coadd these observations of two different resolutions. However, we have used the 2002 F2 data to check for systematic differences in the spectral fits caused by the two different grisms, and we found that the resulting parameters show no systematic difference. Therefore, we can confidently consider our F1 and F2 observations from these two grisms together.

We have reduced and flux calibrated our final F2 and F1 data self-consistently using the IDL based XIDL pipeline<sup>7</sup>. This consistency further limits potential systematics that could be introduced through using the final spectra from Kalirai et al. 2005 (hereafter K05), where the Keck F1 mask observations were first presented. In K05 the original F2 data from 2002 were also presented but were of too low S/N for detailed analysis. For completeness, we note that four white dwarfs from K05 are not presented here. The first being WD11, where its placement on the extreme edge of the F1 mask caused its spectrum to lose everything blueward of  $\sim 4000 \text{ \AA}$ . Similarly, WD3, WD4, and WD7 were the white dwarfs observed only by Gemini/GMOS, which has limited blue sensitivity. For all four of these white dwarf observations,  $\text{H}\epsilon$  and  $\text{H}8$  were not available, and because these are the lines most sensitive to gravity we have concluded these were not suitable for our current study.

Across both LRIS masks we have acquired spectra for 20 white dwarf candidates that have sufficient S/N to analyze. One of these candidates, WD8, appears to be consistent with a main sequence field dwarf. The remaining 19 were found to be real white dwarfs, 14 of which have high enough signal to reliably determine both initial and final masses and cluster membership.

<sup>6</sup> The 2002 data were taken from the public Keck Observatory Archive.

<sup>7</sup> Available at <http://www.ucolick.org/~xavier/IDL/>

### 3. SPECTROSCOPIC WHITE DWARF ANALYSIS

We simultaneously fit the five Balmer lines in each spectrum using the recent models of Tremblay et al. (2011). The automated fitting technique is based on that described by Bergeron et al. (1992), where each line profile is normalized by two defined continua regions surrounding each line. This prevents uncertainties in the fit due to flux calibration. Based on the methods of Levenberg-Marquardt (Press et al. 1986), the final fits are determined by minimizing the  $\chi^2$  when simultaneously considering both  $T_{\text{eff}}$  and  $\log g$ . Combination in quadrature of the resulting internal error and the external uncertainties from the data calibration, estimated at 1.2% in  $T_{\text{eff}}$  and 0.038 dex in  $\log g$  (Liebert, Bergeron, & Holberg 2005), are used to estimate our final uncertainties. These final results and errors are presented in Table 1<sup>8</sup>.

Applying each of the final  $T_{\text{eff}}$  and  $\log g$  to the cooling models for a carbon/oxygen core composition with a thick hydrogen layer by Fontaine et al. (2001) gives the mass, absolute V magnitude, intrinsic B-V color, and white dwarf cooling age. This composition is appropriate for white dwarfs in this range of  $T_{\text{eff}}$  and mass, and Tremblay & Bergeron (2008) observationally estimate that  $\sim 85\%$  of DA white dwarfs cooler than 30,000 K have a thick hydrogen layer. Therefore, these spectroscopic masses provide a direct measurement of the white dwarf's current mass independent of any other assumptions or observational parameters.

We should consider the S/N (per resolution element) and the resulting errors for our white dwarfs (see Table 1). The WD12, WD14, WD15, WD19, and WD23 spectra have low S/N and mass errors greater than 0.1  $M_{\odot}$ . Therefore, their parameters are presented for reference but have been cut from our final analysis. This is because not only are their membership determinations unreliable, but their large mass errors and more importantly their dramatically increasing cooling age uncertainties limit their application to the IFMR.

### 4. WHITE DWARF CLUSTER MEMBERSHIP

To learn the formation history of these white dwarfs, we must first consider their membership of NGC 2099. The membership is based on our spectroscopic white dwarf parameters in comparison to the observed photometry and the adopted cluster parameters. For this study we adopt the photometry and cluster parameters from K01, which are  $E(B-V)=0.21\pm 0.03$ ,  $(m-M)_V=11.55\pm 0.13$ , an age of 520 Myr, and a solar metallicity. This cluster does have a rich history of photometric analysis, and in the Appendix we discuss the multiple studies covering NGC 2099 from the past 20 years and the justification of our adopted parameters. However, in summary, the reddening and age have the most significant variation across the 11 studies (see Table 3 in the Appendix). It is challenging to explain the full variation in determined reddenings ( $E(B-V)$  from 0.21 to 0.3), but the effects of differing adopted metallicity, differing isochrones, and that most studies did not ac-

count for the B-V dependence of reddening (see Fernie 1963 and Twarog et al. 1997) can explain much of it. The large variation in ages (320 to 650 Myr) can be explained by the systematic differences between the adopted isochrones in each of the studies, with a minor dependence on the difference in adopted reddening and metallicity. In Figure 1 we illustrate three of these important isochrones by fitting the K01 photometry and applying their cluster reddening, distance modulus, and metallicity with the applied color dependence of reddening from Fernie (1963). The left panel shows our 520 Myr fit using isochrones from Ventura et al. (1998), the middle panel shows a 540 Myr fit using the PARSEC isochrones from Bressan et al. (2012) using version 1.2S, and the right panel shows a 445 Myr fit using isochrones from Girardi et al. (2000). This shows that the Girardi et al. (2000) isochrones and the very similar Bertelli et al. (1994) isochrones find systematically younger cluster ages, and the  $\sim 0.06$  increase in the B-V color separation of the turnoff and red clump illustrates why many studies must adopt a higher reddening to fit the observed turnoff with these two isochrones.

Table 2 presents the coordinates of our observed white dwarf candidates and the parameters used for analyzing cluster membership. We first directly compare the observed V magnitude for these white dwarfs to their theoretical absolute magnitude. With such a large white dwarf sample from a single cluster, we can comment on the apparent distance modulus. In the left panel of Figure 2, we plot the distribution with  $1\sigma$  error bars of apparent distance modulus for each white dwarf. This is independent of our adopted cluster parameters, and we find a majority of the white dwarfs are consistent. This is based on considering the combination in quadrature of the observed and theoretical magnitude errors ( $1\sigma$ ), and we define outliers as those that are more than  $2\sigma$  from the final sample mean, which is  $(m-M)_V=11.69\pm 0.18$  (solid vertical line). In Figure 2 we have ordered the white dwarfs accordingly where the top 11 are those with consistent distance moduli, the following 3 (WD1, WD20, and WD21) are inconsistent and suggest non-membership, and the final 5 are the low S/N white dwarfs shown for comparison. This white dwarf based distance modulus is consistent with our adopted value of  $(m-M)_V=11.55\pm 0.13$ , and based on the color dependence of reddening and hence extinction, this agreement improves because a moderately larger value ( $11.58\pm 0.13$ ; the dashed vertical line) is expected for the very blue white dwarfs (see discussion of the color dependence of reddening and extinction in the Appendix). The errors of these distance moduli are illustrated at the top of Figure 2.

In the right panel of Figure 2, we similarly plot the distribution of apparent reddenings for each white dwarf based on the difference between the theoretical and observed color. We test for color outliers by considering again the combination in quadrature of the observed and theoretical color errors ( $1\sigma$ ), and outliers are those that are more than  $2\sigma$  from the final sample mean, which is  $E(B-V)=0.265\pm 0.05$  (solid vertical line). Remarkably consistent to the magnitude comparison, we find that all white dwarfs with consistent distance moduli also have consistent reddenings, while one of the three white dwarfs with inconsistent distance moduli also has inconsistent

<sup>8</sup> Relative to K05, our adoptions of hot vs. cool models around the maximum strength of the Balmer lines at  $T_{\text{eff}} = 13,000$  K have changed for WD1, WD9, and WD17.

TABLE 1 - Initial and Final Parameters

ID	$T_{\text{eff}}$ (K)	$\log g$	$M_{WD}$ ( $M_{\odot}$ )	$t_{\text{cool}}$ (Myr)	$M_i$ ( $M_{\odot}$ )	$M_{i470}$ ( $M_{\odot}$ )	$M_{i570}$ ( $M_{\odot}$ )	S/N
NGC 2099 Likely Single Star White Dwarf Members								
WD18	24900±600	8.21±0.06	0.76±0.036	44 <sup>+11</sup> <sub>-10</sub>	3.00 <sup>+0.03</sup> <sub>-0.02</sub>	3.12	2.90	73
WD2	22200±650	8.24±0.07	0.77±0.045	81 <sup>+18</sup> <sub>-16</sub>	3.09 <sup>+0.04</sup> <sub>-0.03</sub>	3.23	2.98	51
WD24	18700±700	8.29±0.11	0.80±0.068	163 <sup>+40</sup> <sub>-35</sub>	3.32 <sup>+0.15</sup> <sub>-0.10</sub>	3.52	3.17	39
WD6	16700±750	8.44±0.11	0.89±0.069	299 <sup>+73</sup> <sub>-62</sub>	3.96 <sup>+0.66</sup> <sub>-0.35</sub>	4.37	3.67	29
WD21	16900±700	8.37±0.11	0.85±0.069	258 <sup>+63</sup> <sub>-52</sub>	3.72 <sup>+0.39</sup> <sub>-0.23</sub>	4.03	3.49	34
WD5	18100±650	8.21±0.01	0.74±0.062	156 <sup>+36</sup> <sub>-32</sub>	3.30 <sup>+0.13</sup> <sub>-0.09</sub>	3.49	3.15	29
WD10	19700±650	8.15±0.09	0.71±0.054	104 <sup>+25</sup> <sub>-22</sub>	3.15 <sup>+0.07</sup> <sub>-0.06</sub>	3.29	3.03	32
WD16	17000±900	8.41±0.15	0.87±0.095	269 <sup>+92</sup> <sub>-70</sub>	3.78 <sup>+0.72</sup> <sub>-0.33</sub>	4.11	3.54	19
WD17	17700±1050	8.56±0.16	0.96±0.099	311 <sup>+116</sup> <sub>-91</sub>	4.05 <sup>+1.34</sup> <sub>-0.52</sub>	4.50	3.74	17
WD13	19900±900	8.47±0.13	0.91±0.082	189 <sup>+57</sup> <sub>-47</sub>	3.42 <sup>+0.24</sup> <sub>-0.16</sub>	3.62	3.25	24
WD9	16200±800	7.95±0.14	0.59±0.078	139 <sup>+47</sup> <sub>-38</sub>	3.25 <sup>+0.16</sup> <sub>-0.11</sub>	3.42	3.11	20
White Dwarfs Inconsistent with Single Star Membership								
WD22	19900±550	8.48±0.07	0.92±0.043	193 <sup>+30</sup> <sub>-27</sub>	–	–	–	61
WD20	19400±650	8.24±0.09	0.76±0.057	131 <sup>+30</sup> <sub>-26</sub>	–	–	–	44
WD1	11100±250	8.22±0.08	0.74±0.051	630 <sup>+94</sup> <sub>-84</sub>	–	–	–	54
Low Signal to Noise White Dwarfs								
WD23	14200±2300	8.36±0.29	0.84±0.180	408 <sup>+356</sup> <sub>-203</sub>	–	–	–	13
WD15	13200±1000	8.50±0.17	0.92±0.110	621 <sup>+285</sup> <sub>-192</sub>	–	–	–	15
WD14	11900±560	8.07±0.19	0.65±0.110	415 <sup>+146</sup> <sub>-102</sub>	–	–	–	16
WD19	20700±2050	8.50±0.30	0.93±0.180	177 <sup>+143</sup> <sub>-92</sub>	–	–	–	9.5
WD12	13400±1300	7.93±0.23	0.57±0.120	250 <sup>+130</sup> <sub>-108</sub>	–	–	–	13

reddening. Due to the relatively large photometric color errors, this test is not as stringent as the magnitude test, but it is still important. This white dwarf based reddening is in agreement with our adopted reddening of  $0.21 \pm 0.03$ , and the agreement improves further because a moderately larger apparent reddening ( $0.22 \pm 0.03$ ; the dashed vertical line) is expected for white dwarfs.

While the numbers are limited, we can also separate the final white dwarfs into their respective F1 and F2 fields to test for potentially large variations in reddening and extinction, which should be considered in clusters of moderate reddening. The difference in each field's mean reddening or distance modulus is not found to be significant ( $\Delta E(B-V) = 0.02 \pm 0.06$ ;  $\Delta(m-M)_V = 0.05 \pm 0.25$ ), and any potential variable reddening is likely not significant within the relatively small FOV of LRIS itself ( $5' \times 7'$ ). Therefore, variable reddening or extinction likely have not affected our membership analysis. We should also note that if we adopt these white dwarf based distance modulus and reddening for our photometric isochrone fits, there is only a moderate effect on the age giving a best fit of 490 Myr adopting the Ventura et al. (1998) isochrones and 510 Myr adopting the Bressan et al. (2012) isochrones ( $\Delta \text{Age} \sim 30$  Myr).

Figure 3 shows the Balmer-line fits to the spectra for these 11 member white dwarfs used in our analysis of NGC 2099. Figure 4 focuses on the photometric characteristics of the observed white dwarfs. Here we have indicated membership, including observed photometric error bars for the final members, and have plotted them relative to a series of white dwarf cooling models of different mass.

In K01 their photometric comparison of white dwarf candidate density within and outside the cluster field found that  $\sim 75\%$  of the white dwarf candidates are cluster members. We find that 11 (73%) of our 14 observed white dwarfs candidates that have S/N appropriate for

membership analysis are consistent with singly evolved NGC 2099 members. This reconfirms the richness of the WD population of NGC 2099 and the high return on its candidate observations, where many of the candidates found in the K01 photometry still remain unobserved.

We have determined cluster membership, and this provides a valuable reference for further analysis of these white dwarfs. The white dwarf cooling age represents the time since that white dwarf formed at the tip of the asymptotic giant branch (AGB). Therefore, direct comparison of a white dwarf's cooling age to its parent cluster's total age gives us the total evolutionary lifetime (to the tip of the AGB) for that white dwarf's progenitor star. We have applied these lifetimes to the models of Hurley et al. (2000) at solar metallicity to determine the ZAMS masses for each progenitor, which can be compared directly to their final observed white dwarf mass. Before continuing, Salaris et al. (2009) noted that inconsistencies between the input physics of isochrones to determine the cluster age and the input physics of the adopted model for determining evolutionary times at specific progenitor masses are not always consistent. However, we find that the progenitor masses found for the stars at the tip of the AGB at a given age are consistent to within 1% for Hurley et al. (2000) and both the Ventura et al. (1998) and Bressan et al. (2012) isochrones at our progenitor mass range.

## 5. INITIAL FINAL MASS RELATION

Our 11 white dwarfs consistent with singly evolved cluster membership span a broad range of masses from 0.59 to  $0.96 M_{\odot}$ . Figure 5 presents the IFMR for the cluster when adopting the age of 520 Myr. For reference, the linear fit IFMR observed by Kalirai et al. (2009; hereafter K09) is plotted with its errors (solid and dashed lines, respectively). This K09 relation is

$$M_{\text{final}} = (0.101 \pm 0.006)M_{\text{initial}} + 0.463 \pm 0.018M_{\odot},$$

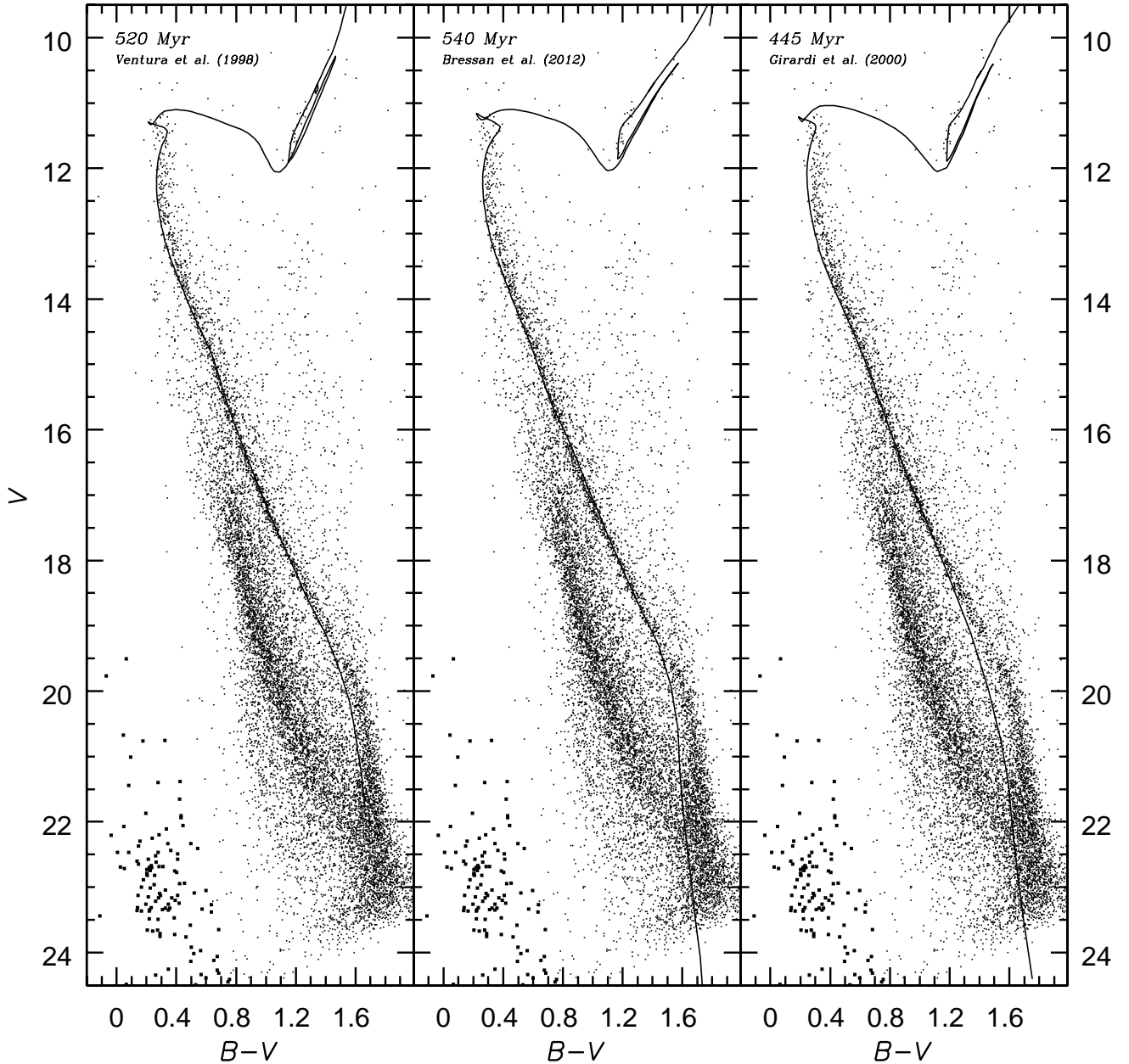


FIG. 1.— We show three panels of isochrone fits of the K01 photometry for NGC 2099, where we have also adopted their photometric parameters but apply a color dependence of the reddening. (The rich white dwarf population is emphasized with bold data points.) The left and middle panels show our age fits using the quite similar Ventura et al. (1998) and Bressan et al. (2012) isochrones. The right panel helps to illustrate the important systematics introduced by adopting the Girardi et al. (2000) isochrones, which are also nearly equivalent to the commonly used Bertelli et al. (1994) isochrones.

which is an update to that of Kalirai et al. (2008) that has additional low-mass data from M4 and updated spectral models more consistent with those adopted here. Additionally, these K09 data include the previous NGC 2099 results from K05 and are based on a large data set spanning a progenitor mass range of  $\sim 1$  to  $6 M_{\odot}$ . In Figure 5 a vertical solid line is shown that represents the ZAMS mass ( $2.91 M_{\odot}$ ) of a star that is currently on the tip of the AGB at 520 Myr. Therefore, under the adopted age and mass-loss rates we cannot reach progenitor masses lower than this in NGC 2099. For our data the white dwarf mass errors are those already described, while the progenitor mass errors are based on the error in white dwarf cooling ages. Because these white dwarfs come from the

same cluster, the error in cluster age is systematic and not shown in these error bars. These progenitor parameters are also presented in Table 1 for direct comparison to their final white dwarf parameters.

Based on the somewhat meaningful variation in white dwarf mass errors (nearly a factor of 3), we present both an unweighted and weighted linear fit to the IFMR for the  $M_{\text{initial}}$  range of 3 to  $4 M_{\odot}$ . Figure 5 presents the weighted linear fit (dotted line) given here

$$M_{\text{final}} = (0.171 \pm 0.057)M_{\text{initial}} + 0.219 \pm 0.187M_{\odot}.$$

For comparison, the unweighted linear fit of these IFMR data is  $M_{\text{final}} = (0.218 \pm 0.067)M_{\text{initial}} + 0.051 \pm 0.234 M_{\odot}$ . Before we compare the coefficients, we should clarify that

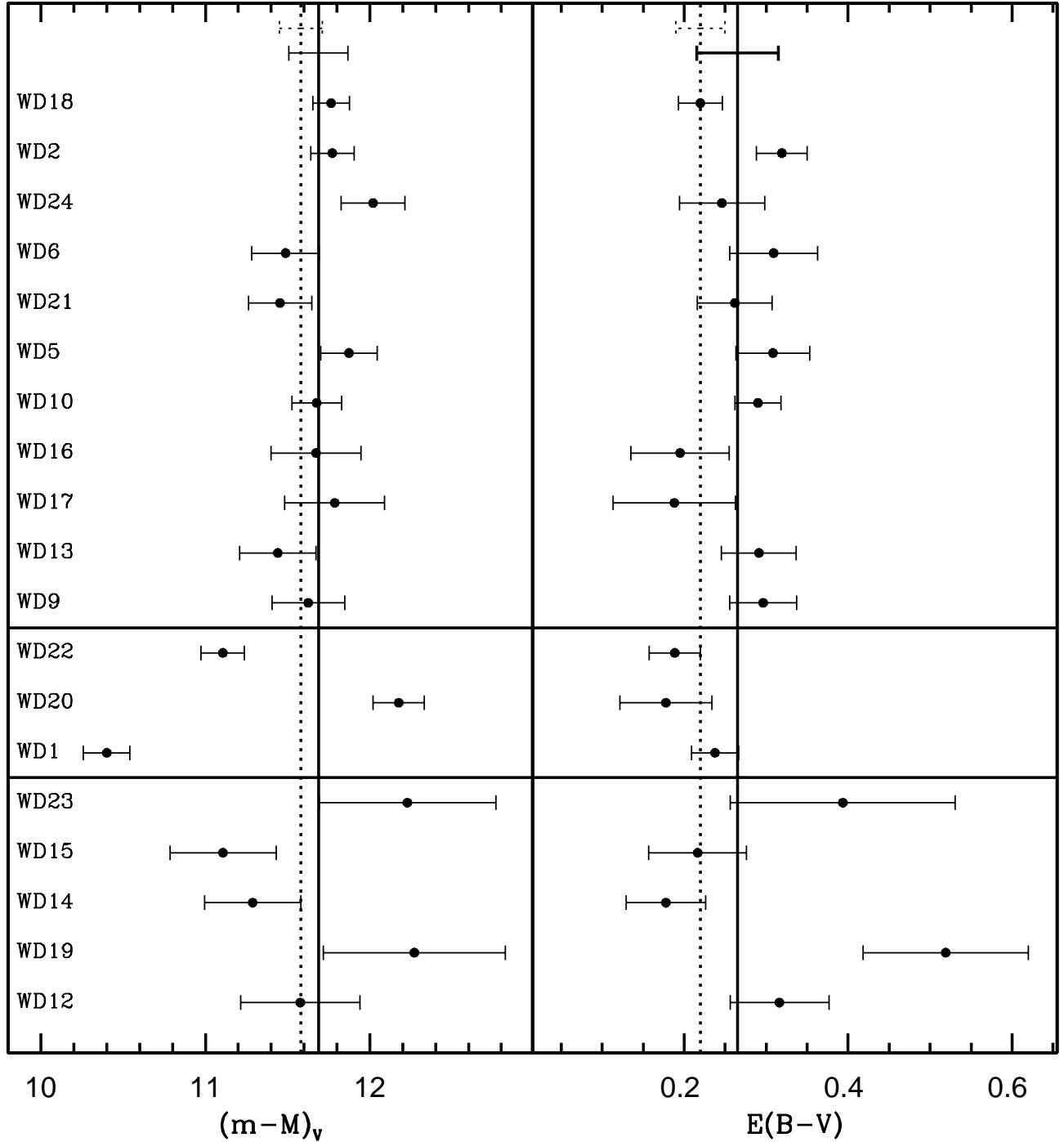


FIG. 2.— In the left panel we display the distribution and  $1\sigma$  error bars for the white dwarf based distance moduli. The upper 11 white dwarfs are consistent (within  $2\sigma$ ) with the mean, and we find the middle 3 are inconsistent. For reference the bottom 5 white dwarfs are those that have been cut for their low S/N. The solid vertical line represents the mean of the member distance moduli and the dashed line is our photometric based distance modulus, with their respective error bars at the top. In the right panel we display the distribution and error bars for the white dwarf based reddening. Assuringly, the 11 white dwarfs with consistent distance moduli also have consistent reddening. Again, the solid vertical line represents the mean of the member reddening, and the dashed line is our photometric based reddening.

the zeropoint error is the result of propagating the slope error to the y-axis, and so they should not be considered independently. Even under this limitation, the weighted and unweighted coefficients are consistent within the errors, but we take the weighted fit as our final result because we feel the discrepant WD9 and WD13 overly influence the slope of the unweighted relation.

WD9 and WD13 are the only two members that are greater than  $1\sigma$  (white dwarf mass error) from the weighted linear fit. WD13 is  $1.35\sigma$  discrepant and WD9 is  $2.42\sigma$  discrepant from the relation. WD13's minor discrepancy is not of significant concern, and its high mass ( $0.91 M_{\odot}$ ) makes it unlikely that it is a field dwarf contaminating our sample. However, WD9 is far more

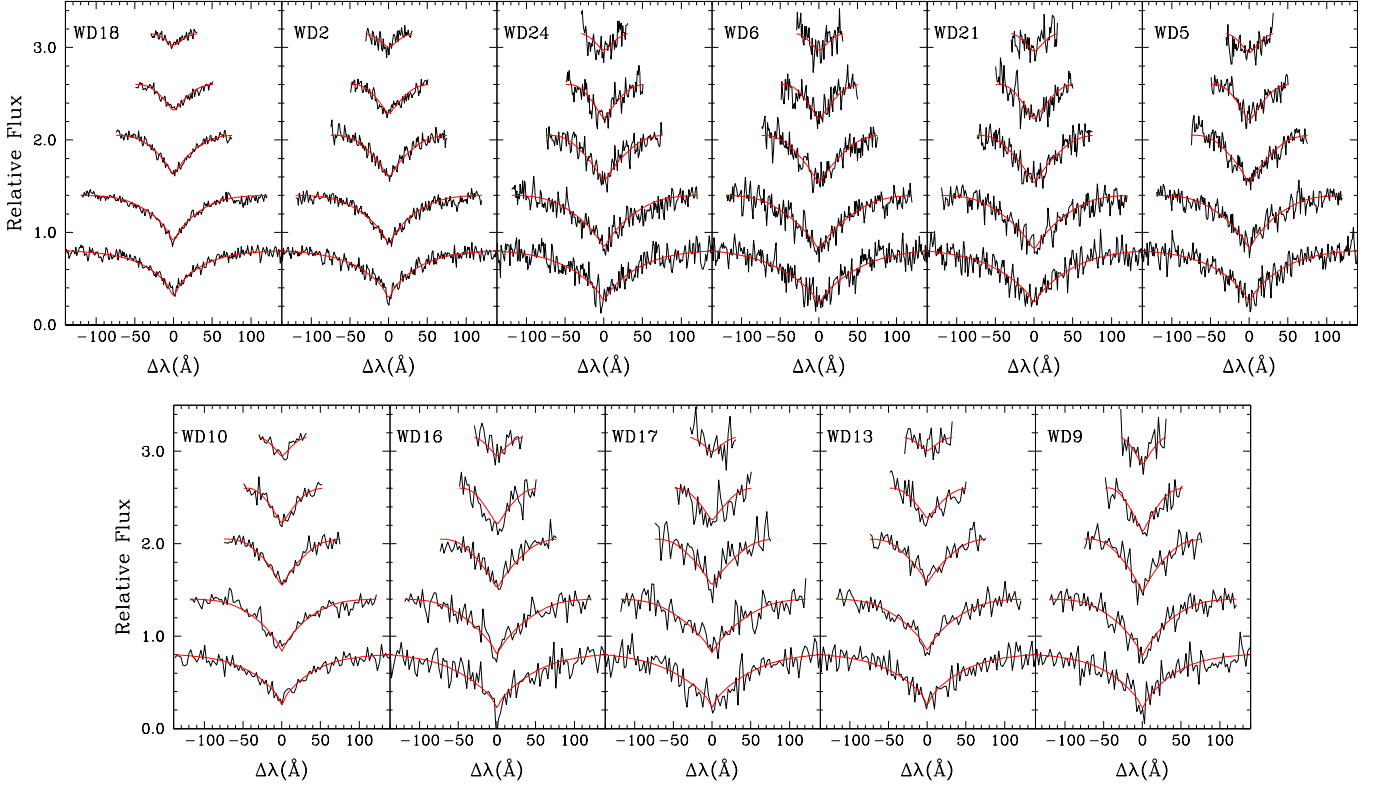


FIG. 3.— The Balmer fits for the 11 final white dwarf members of NGC 2099. The  $H\beta$ ,  $H\delta$ ,  $H\gamma$ ,  $H\epsilon$ , and  $H8$  fits are shown from bottom to top. The upper 6 white dwarf spectra are from the F2 mask and the bottom 5 white dwarf spectra, which have been binned for display, are from the F1 mask.

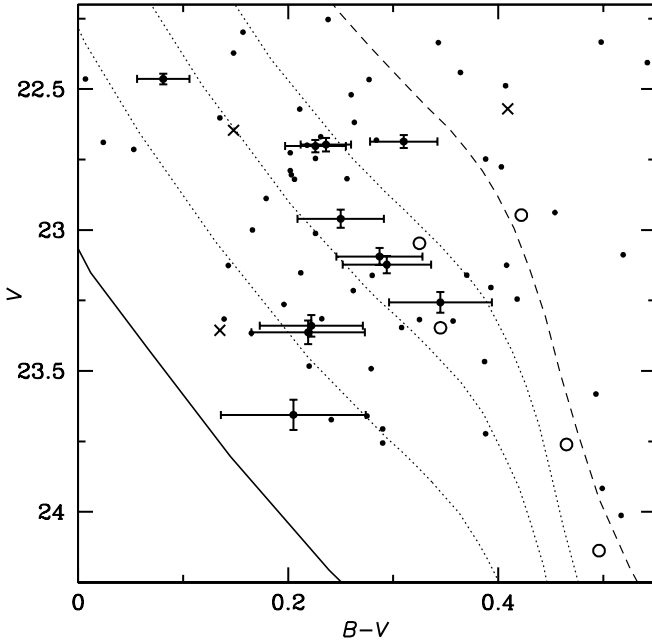


FIG. 4.— The white dwarf photometry where we differentiate between observed non-members (x's), likely singly evolved members (solid circle), observed white dwarfs with low S/N (open circles), and unobserved candidates (small points). White dwarf cooling models are plotted for reference from left to right of  $1.2 M_{\odot}$  (solid line),  $1.0$ ,  $0.8$ , and  $0.6 M_{\odot}$  (dotted lines), and  $0.4 M_{\odot}$  (dashed line). The mean distance modulus and reddening derived from these white dwarf members are used on these cooling models.

discrepant, and its low mass ( $0.59 M_{\odot}$ ) is more difficult to explain, where when assuming standard stellar evolu-

tion a progenitor star that would create a white dwarf of this mass would take several Gyr to fully evolve. The effects of a binary companion could possibly explain the significant mass loss that would be required to create this white dwarf, but no evidence for a binary companion was found in its magnitude and color analysis. It is more probable that this white dwarf is simply contaminating our cluster membership sample rather than it being indicative of any significant variation of the mass-loss history of a singly evolved star at progenitor mass of  $3.25 M_{\odot}$ . Its low white dwarf mass is also comparable with field white dwarf expectations, where the mean mass of white dwarfs in the SDSS DR7 sample is  $0.598 M_{\odot}$  (at  $T_{\text{eff}} > 13,000 \text{ K}$ ; Kleinman et al. 2013). We do not remove WD9 or WD13 from our final sample, but due to their higher errors, their effect on the final weighted relation is minimal.

Besides these two white dwarfs, this weighted linear relationship describes the remaining 9 member white dwarfs very well and the errors can fully explain the observed spread in the IFMR. Therefore, within this single cluster, there is no convincing evidence for stochastic mass loss that could explain the large scatter in the IFMR typically observed when combining data from multiple studies.

Lastly, in Figure 5 the effects of cluster age errors on progenitor mass are illustrated. The younger cluster age (470 Myr) is represented by inverted triangles and the older cluster age (570 Myr) is represented by triangles. This shows that in the lower-mass white dwarfs ( $0.7$  to  $0.8 M_{\odot}$ ) the progenitor masses are only moderately affected by adopting a 50 Myr older or younger cluster

TABLE 2 - Membership Test

ID	Field	$\alpha$ (J2000)	$\delta$ (J2000)	$\nabla$ (Theory)	$\nabla$ (Obs.)	B-V (Theory)	B-V (Obs.)	$t_{cool}$ (Myr)
NGC 2099 Likely Single Star White Dwarf Members								
WD18	F2	5:52:13.32	32:28:55.9	22.39±0.11	22.464±0.019	0.126±0.009	0.081±0.025	44 <sup>+11</sup> <sub>-10</sub>
WD2	F2	5:52:17.54	32:29:03.4	22.62±0.13	22.702±0.022	0.172±0.011	0.226±0.029	81 <sup>+18</sup> <sub>-16</sub>
WD24	F2	5:52:25.34	32:29:35.2	23.01±0.19	23.340±0.038	0.241±0.017	0.222±0.049	163 <sup>+40</sup> <sub>-35</sub>
WD6	F2	5:52:18.44	32:29:37.6	23.46±0.20	23.257±0.037	0.301±0.022	0.345±0.049	299 <sup>+73</sup> <sub>-62</sub>
WD21	F2	5:52:26.42	32:30:04.3	23.33±0.19	23.094±0.030	0.290±0.020	0.287±0.041	258 <sup>+63</sup> <sub>-52</sub>
WD5	F2	5:52:25.46	32:30:54.4	22.94±0.17	23.123±0.031	0.251±0.016	0.294±0.042	156 <sup>+36</sup> <sub>-32</sub>
WD10	F1	5:52:25.82	32:36:03.8	22.71±0.15	22.697±0.024	0.211±0.014	0.236±0.024	104 <sup>+25</sup> <sub>-22</sub>
WD16	F1	5:52:22.89	32:36:29.4	23.38±0.27	23.363±0.042	0.289±0.026	0.219±0.054	269 <sup>+92</sup> <sub>-72</sub>
WD17	F1	5:52:29.29	32:37:06.7	23.56±0.30	23.656±0.054	0.282±0.029	0.205±0.069	311 <sup>+116</sup> <sub>-91</sub>
WD13	F1	5:52:16.21	32:38:18.5	23.21±0.23	22.960±0.032	0.224±0.020	0.250±0.041	189 <sup>+57</sup> <sub>-47</sub>
WD9	F1	5:52:25.14	32:40:03.6	22.75±0.22	22.686±0.023	0.279±0.025	0.310±0.032	139 <sup>+47</sup> <sub>-38</sub>
White Dwarfs Inconsistent with Single Star Membership								
WD22	F2	5:52:04.99	32:25:40.6	23.23±0.13	22.646±0.023	0.224±0.012	0.148±0.029	193 <sup>+30</sup> <sub>-27</sub>
WD20	F2	5:52:12.88	32:29:50.0	22.87±0.15	23.356±0.044	0.222±0.015	0.135±0.054	131 <sup>+30</sup> <sub>-26</sub>
WD1	F1	5:52:26.80	32:30:46.7	23.86±0.14	22.570±0.020	0.437±0.006	0.409±0.028	630 <sup>+94</sup> <sub>-84</sub>
Low Signal White Dwarfs and a Non White Dwarf								
WD23	F2	5:52:03.30	32:27:30.4	23.60±0.53	24.138±0.090	0.367±0.061	0.496±0.123	408 <sup>+356</sup> <sub>-203</sub>
WD8	F2	5:52:15.87	32:27:53.4	–	21.655±0.011	–	0.421±0.016	–
WD15	F1	5:52:27.42	32:35:50.0	23.93±0.32	23.347±0.042	0.394±0.021	0.345±0.056	621 <sup>+285</sup> <sub>-192</sub>
WD14	F1	5:52:06.43	32:38:29.4	23.45±0.29	23.047±0.034	0.412±0.015	0.325±0.046	415 <sup>+146</sup> <sub>-102</sub>
WD19	F1	5:52:01.12	32:39:50.4	23.18±0.55	23.761±0.067	0.211±0.043	0.465±0.091	177 <sup>+143</sup> <sub>-92</sub>
WD12	F1	5:52:11.96	32:40:39.5	23.06±0.36	22.947±0.032	0.371±0.041	0.422±0.044	250 <sup>+130</sup> <sub>-108</sub>

age. However, the higher-mass stars with more rapid evolutionary times are increasingly more sensitive to the adopted cluster age. Therefore, the younger cluster age finds a slightly shallower IFMR, but the older cluster age further increases its slope.

Our final weighted IFMR for our analyzed mass range ( $M_{\text{initial}}$  of  $\sim 3$  to  $4 M_{\odot}$ ) is steeper than the linear relation from K09 based on a much broader sample ( $M_{\text{initial}}$  of  $\sim 1$  to  $6 M_{\odot}$ ). This suggests that a linear relation is insufficient to describe this full mass range. It is also important to clarify, however, that we are comparing to the final linear IFMR fit in K09, but their white dwarf data itself do indicate possible nonlinearity across their full mass range. In particular, for our mass range analyzed in this current study the K09 data suggested a possibly steeper IFMR slope in this region followed by a shallower slope at higher masses, but as discussed in Kalirai et al. (2008) their errors and numbers were too limited for a convincing nonlinear fit. Similar to K09, other recent IFMR studies have also considered the possible nonlinearity in the IFMR, but a majority of these have stated that their errors, which resulted primarily from systematics between the differing studies and clusters considered, were too significant to justify a nonlinear fit. For comparison, Ferrario et al. (2005) linearly fit their data spanning  $M_{\text{initial}}$  of 2.5 to  $6.5 M_{\odot}$  with a slope of  $0.10038 \pm 0.00518$  and a y intercept of  $0.43443 \pm 0.01467$ , very similar to the relation from K09. Salaris et al. (2009) linearly fit their data approximately spanning  $M_{\text{initial}}$  of 1.7 to  $7 M_{\odot}$  with a slope of 0.084 and a y intercept of 0.466. Williams et al. (2009) span the same mass range and find a linear fit with slope of  $0.129 \pm 0.004$  and y intercept of  $0.339 \pm 0.015$ . All of these fits are comparable to K09.

Previous evidence in support of a turnover in the IFMR at higher progenitor masses is primarily theoretical. In

both IFMR models by Marigo & Girardi (2007) and Meng et al. (2008) a turnover in the slope of the IFMR is predicted near a progenitor mass of  $\sim 4 M_{\odot}$ . Meng et al. (2008) describe this turnover as a result of only these higher-mass stars undergoing a second dredge-up event during their AGB evolution, which reduces their core mass. Previous observational evidence for this turnover is found in Dobbie et al. (2012), where they observed seven white dwarf members of NGC 3532 spanning progenitor masses of  $\sim 3.5$  to  $6 M_{\odot}$ . Similar to our current work, their focus on a single rich cluster prevented systematics that could be the source of any of features in their IFMR. While their numbers were still too limited to be able to define two independent slopes both above and below this  $\sim 4 M_{\odot}$  turning point, the data do suggest a turnover exists near this  $M_{\text{initial}}$ .

To further analyze this mass range, in Figure 6 we compare to the large sample of 18 bright and well studied white dwarfs from the metal-rich Hyades and Praesepe ( $[\text{Fe}/\text{H}] = +0.11 \pm 0.01 (\pm 0.03)$  and  $+0.16 \pm 0.05 (\pm 0.03)$ , respectively; Carrera & Pancino 2011). The Hyades and Praesepe single white dwarfs have been analyzed using consistent techniques and models and are taken from the sample of Kalirai et al. 2014. Similar to our NGC 2099 data we fit the initial and final masses of these 18 Hyades and Praesepe white dwarfs using a linear relationship that well characterizes the data across this mass range. We also overplot our final sample of white dwarfs from NGC 2099. In comparison, the Hyades and Praesepe white dwarfs span a comparable mass range to NGC 2099, but the two older clusters extend to even lower masses. The linear relations are remarkably consistent with nearly identical slopes and no meaningful offset. This consistency suggests that in this mass range and across the metallicity range of these three clusters ( $0 \lesssim [\text{Fe}/\text{H}] \lesssim 0.15$ ) there is no significant metallicity de-

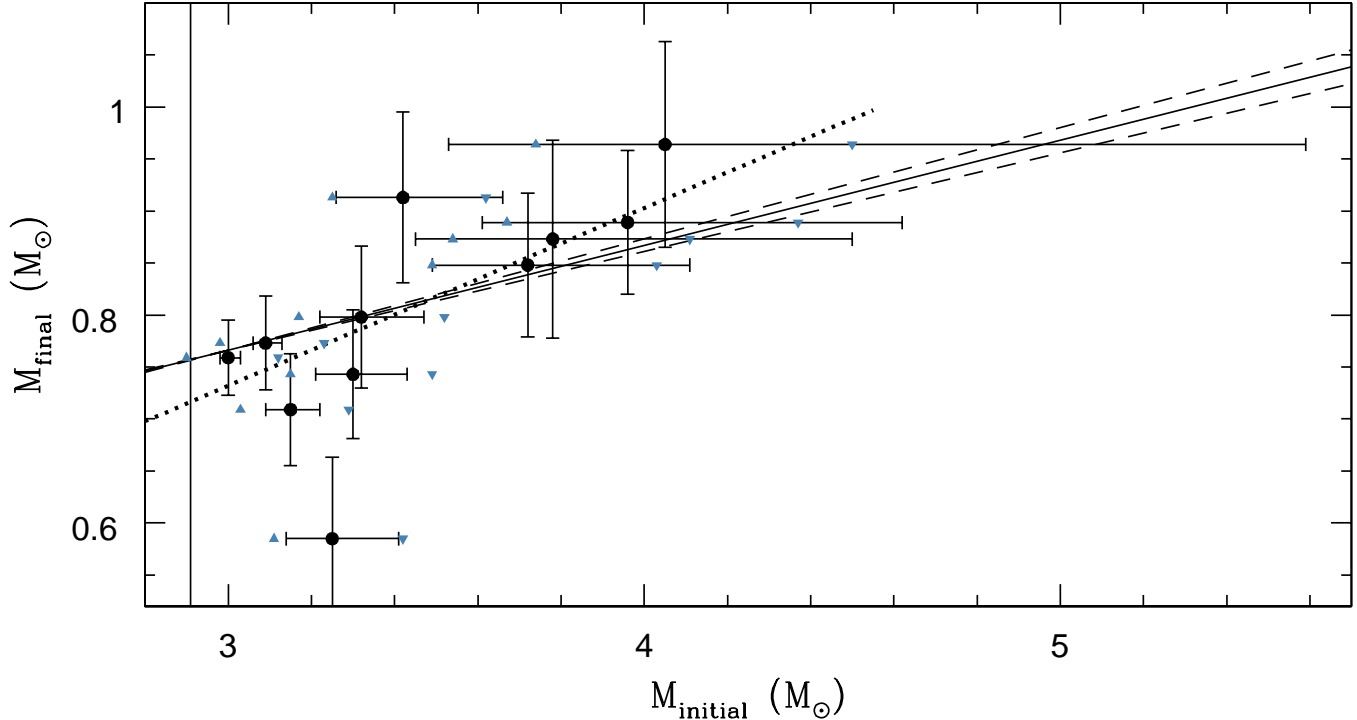


FIG. 5.— The IFMR relation for our cluster members, adopting a cluster age of 520 Myr. The linear IFMR is from K09 (solid line) with its errors (dashed lines). The steeper slope of our linear NGC 2099 IFMR fit (dotted line) is shown. The solid vertical line represents the current progenitor mass at the tip of the AGB. To illustrate the effects of adopted age on our final sample, the progenitor masses based on a 470 Myr cluster age are shown by inverted gray triangles and the progenitor masses based on a 570 Myr cluster age are shown by gray triangles.

pendence in the IFMR. This is also qualitatively consistent with both the metallicity dependent IFMR models by Marigo & Girardi (2007) and Meng et al. (2008), where there are no meaningful differences ( $\Delta M_{\text{final}} < 0.01 M_{\odot}$ ) predicted at these masses across this specific metallicity range.

The observed consistency between the different samples also can improve our statistics by combining the full sample of 29 white dwarfs. This gives our final combined linear relation across the  $M_{\text{initial}}$  range of 3 to 4  $M_{\odot}$  of  $M_{\text{final}} = (0.163 \pm 0.022)M_{\text{initial}} + 0.238 \pm 0.071 M_{\odot}$ . Direct comparison to the linear relation fit in K09 illustrates that the steeper slope observed in this mass range for our data is now far more significant and also meaningfully steeper than the linear IFMR relations found in Ferrario et al. (2005), Salaris et al. (2009), and Williams et al. (2009). This further indicates that the full mass range of the IFMR cannot simply be represented by a linear relation.

## 6. SUMMARY

We have spectroscopically observed 20 white dwarf candidates in the rich open cluster NGC 2099. We have focused on this single open cluster to limit the potential systematic effects of combining white dwarf data from multiple open clusters, which may be the driving cause of the large scatter observed in the IFMR. The rich turnoff and red giant clump of NGC 2099 also allows for a reliable determination of cluster parameters. However, to understand the systematic parameter differences that remain in the literature, in the Appendix we have considered the color dependence of reddening, the effects of metallicity, and the systematic differences between the

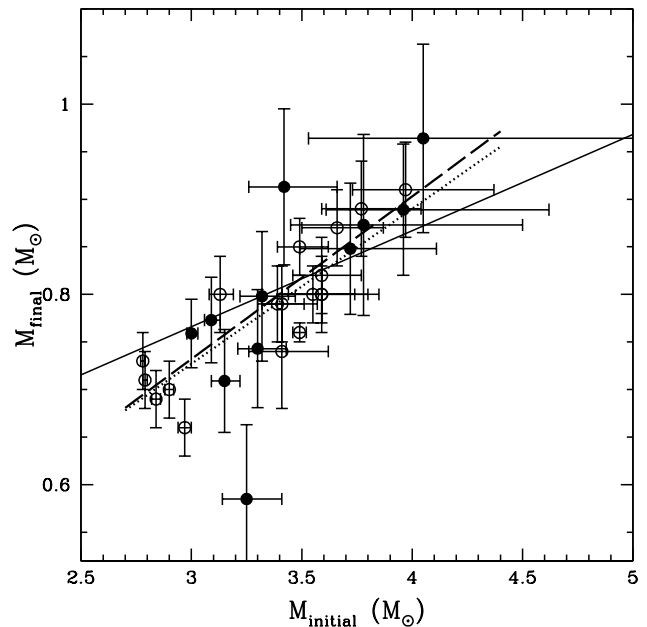


FIG. 6.— We compare our final sample from NGC 2099 (solid points) and its linear fit (dashed line) to the white dwarf sample of the Hyades and Praesepe (open circles) with its linear fit (dotted line). The slopes are nearly identical and with only an insignificant offset. As in Figure 5, the shallower K09 IFMR is shown in comparison (solid line) but without its errors for additional clarity.

adopted isochrones used to analyze this cluster.

With our spectroscopic parameters determined for the observed white dwarfs, and after appropriate cuts based on spectra with large errors, we find that 11 of 14 of the well characterized white dwarfs are consistent with sin-

gle star cluster membership. This is a high percentage relative to the field and is consistent with the photometric prediction made by K01, and this further emphasizes the richness of this cluster. With this rich white dwarf cluster population, we have been able to independently test the photometrically determined cluster parameters of distance modulus and reddening, and both methods give consistent values. This further strengthens our adopted cluster age of 520 Myr.

Applying a 520 Myr age to the 11 cluster white dwarfs provides a well sampled single cluster IFMR that spans a white dwarf mass of  $\sim 0.7$  to  $0.95 M_{\odot}$ , excluding a low-mass outlier, which corresponds to progenitor masses of  $\sim 3$  to  $4 M_{\odot}$ . In general with our white dwarfs, the observational errors can account well for the observed spread relative to a weighted linear fit IFMR. This suggests that stochastic mass loss is not likely a significant contributor to the spread in the observed IFMR when multiple studies are combined. The slope for this weighted linear IFMR spanning initial masses of  $\sim 3$  to  $4 M_{\odot}$  is found to be steep relative to the linear IFMR adopted over a much broader mass range in K09.

Comparison of this relation to that found in white dwarfs of the metal-rich Hyades and Praesepe clusters finds remarkable consistency. This not only is in agreement with theoretical predictions for metallicity dependence of the IFMR, but considering together this large sample of 29 white dwarfs more reliably establishes the empirical IFMR for progenitors of 3 to  $4 M_{\odot}$ . This final relation provides stronger observational evidence that a nonlinear IFMR, with a shallower slope in higher mass, may better represent the full mass range. This plateauing of the relation at higher masses further exacerbates the current difficulties in determination of the high-mass IFMR (white dwarf masses  $\gtrsim 1 M_{\odot}$ ), where there are currently only a limited number of white dwarfs of which all have large errors. Therefore, new and higher-mass white dwarfs must be discovered because extrapolation beyond the current data poorly estimates both mass-loss rates and final masses for progenitor stars at  $>4 M_{\odot}$ .

This project was supported by the National Science Foundation (NSF) through grant AST-1211719. P-E.T. was supported during this project by the Alexander von Humboldt Foundation and by NASA through Hubble Fellowship grant HF-51329.01, awarded by the Space Telescope Science Institute, which is operated by the Association of Universities for Research in Astronomy, Incorporated, under NASA contract NAS5-26555. Lastly, we thank the referee for the thorough and very helpful report.

## APPENDIX

## CLUSTER PARAMETERS

The cluster parameters of NGC 2099 (M37) play an important role in our analysis, and the cluster age, distance modulus, and metallicity need to be considered. In Table 3 we list the published literature values for the cluster parameters from the past 20 years. The determination of all three of these parameters are typically interrelated and also have a strong dependence on the adopted cluster reddening, which we discuss first.

*Reddening*

The reddening for this cluster is moderate, and its past measurements have typical found two ranges:  $E(B-V) = 0.21$  to  $0.23$  and a higher set of values of  $0.27$  to  $0.30$ . These reddenings are based on fits of theoretical isochrones or of the empirical Hyades main sequence to NGC 2099 photometry, which are typically of only one or two colors. In three cases the photometry does not reach deep enough to reliably define the main sequence below the turnoff (Mermilliod et al. 1996, Twarog et al. 1997, and Kiss et al. 2001). While the isochrones adopting higher reddening do fit the turnoff of NGC 2099 well, their fit of the rich population of red clump giants is poor. The one exception being Nilakshi & Sagar (2002;  $E(B-V)=0.30$ ), but they had to adopt a very metal-poor isochrone ( $Z=0.008$ ) to fit both the turnoff and red clump well. Conversely, isochrones that adopt the lower reddening values do noticeably better with the giants and still provide a reasonable but typical too blue of a fit to the turnoff.

This difficulty of fitting an isochrone simultaneously to both the turnoff and red clump has been noted in most previous studies for NGC 2099. This may be indicative of an issue caused by the typically assumed solar metallicity or the adopted input physics of the isochrones. For example, comparing the similar Ventura et al. (1998) and Bressan et al. (2012) isochrones to the older Padova group isochrones of Girardi et al. (2000) and Bertelli et al. (1994) (see Figure 1) we do find that for the respective best fits the color difference between the turnoff and red clump is  $\sim 0.06$  greater in  $B-V$  for the latter two isochrones. A majority of this increase is caused by their isochrones predicting a bluer turnoff, which may explain why studies that adopt these models also adopt higher reddenings because it is needed to match the observed turnoff, but as stated this gives a poor red clump fit.

The narrower color separation found for the Ventura et al. (1998) and Bressan et al. (2012) isochrones still has difficulty fitting the turnoff and red clump simultaneously, but this may be explained by the moderate reddening of NGC 2099. The observed reddening is increased in bluer stars, and when using the relation from Fernie (1963) the reddening for the turnoff is approximately 10% higher than that found for the red clump. At the moderate reddening for NGC 2099 this factor is no longer insignificant and this diminishes the apparent color difference between the turnoff and red clump further by  $0.02$  to  $0.03$ . Twarog et al. (1997) also discussed the importance of this color dependence on the reddening for these different groups of stars from NGC 2099. Correcting for this greatly improves the simultaneous fit of both the turnoff and red clump seen in Figure 1 when adopting the K01 reddening of  $E(B-V)=0.21\pm 0.03$ , which we adopt in this paper. Lastly, to lend further credence to the lower reddenings, private communication with A. Steinhauer (2013) gives that they find an  $E(B-V)$  of  $0.22$ . Their deep multi-color UBVR photometry of NGC 2099 provides a stronger constraint on the cluster reddening, with the reddening sensitive U photometry in particular.

*Metallicity*

The cluster metallicity is quite reddening dependent, both photometrically and spectroscopically. A majority of past photometric publications have simply assumed solar metallicity for their isochrone fits. While a handful of photometric metallicity estimates exist, there is large variation ( $[Fe/H] \sim -0.2$  to  $0.09$ ) and great uncertainty. Spectroscopically measured  $[Fe/H]$  are limited for this cluster, but Pancino et al. (2010) derived  $[Fe/H]=+0.01\pm 0.05(\pm 0.10)$  from 3 giants when adopting  $E(B-V)=0.27$  for their color- $T_{\text{eff}}$  relation. In contrast, A. Steinhauer (private communication 2013) derived a spectroscopic  $[Fe/H]$  of  $-0.136\pm 0.028\pm \text{systematics}$  from 20 main sequence stars using their lower reddening of  $E(B-V)=0.22$ . Considering the reddening uncertainty and the corresponding systematic abundance error, these metallicities are still consistent. Reassuringly, when adopting this lower reddening for redetermining the  $T_{\text{eff}}$  for the sample from Pancino et al. (2010), a remarkably consistent  $[Fe/H]$  of  $-0.115$  is found. Therefore, when adopting a smaller reddening as we have, both studies find that this cluster is consistent with slightly subsolar, and when adopting the higher reddening it is approximately solar. In regard to our comparison to the metal-rich Hyades and Praesepe, a significant reddening of  $0.33$  would have to be adopted to give NGC 2099 a consistent high metallicity. While uncertainty does remain, variations of our adopted metallicity from  $[Fe/H]=-0.1$  to solar do not meaningfully affect our results. For this paper we continue to adopt solar metallicity for NGC 2099.

*Distance Modulus*

Distance modulus also plays an important role in our white dwarf membership analysis. However, unlike the other cluster parameters, a relatively strong consistency is found across previous studies. Only in the case of Salaris et al. (2009) is it moderately different, where their high distance modulus is the result of the adopted metal-rich isochrone in combination with high reddening. Here, we adopt the distance modulus from K01 of  $(m-M)_V=11.55\pm 0.13$ , which based on the range in the literature is appropriate.

## Age

The age of NGC 2099 from isochrone fits is the cluster parameter with the most significant variation found in the previous literature. However, a majority of this dispersion found in ages is simply the result of the adopted isochrones, where the adopted isochrone in each study is listed in the notes of Table 3. We can first discuss isochrones without convective overshooting, which as is discussed in K01 are found to not reliably fit the features of the upper main sequence, and these types of models also give significantly younger turnoff/giant fits. Salaris et al. (2009) also found similar issues with models that did not include overshoot. From the studies in Table 3, only Hartman et al. (2008) used isochrones without overshoot (An et al. 2007) and found a 485 Myr age, but when they fit the Yi et al. (2001; hereafter Y<sup>2</sup>) isochrones with overshoot they found an age of 580 Myr.

Before we begin our systematic comparison of isochrones with overshoot, we note that each isochrone set has its own adoption of  $Z$  for solar metallicity. The Bertelli et al. (1994) and Ventura et al. (1998) isochrones adopted  $Z=0.020$  for solar, Pietrinferni et al. (2004) adopted  $Z=0.0198$ , Girardi et al. (2000) adopted  $Z=0.019$ , and Y<sup>2</sup> adopted  $Z=0.018$ . Systematic differences introduced by this variation are negligible and for our solar metallicity isochrones we adopt that from each paper. However, the recent Bressan et al. (2012) PARSEC isochrones adopted a significantly lower  $Z=0.0152$  for solar metallicity. Therefore, for our comparisons we have adopted  $Z=0.019$  for their models. We note that this does cause their isochrone G dwarfs to be systematically redder (see the central panel of Figure 1), but otherwise this provides a more appropriate comparison for systematic differences between these isochrones.

The Bertelli et al. (1994) and Girardi et al. (2000) isochrones have been commonly used in the literature age measurements. Both of these sets of isochrones are from the Padova group, and direct comparison of these models at a range of cluster parameters similar to that of NGC 2099 find that they are nearly equivalent. Similarly, the isochrones of Pietrinferni et al. (2004) were used in Salaris et al. (2009), and Salaris et al. found that the cluster ages derived from these models have no systematic difference to those of Girardi et al. (2000). These three are considered our first group of isochrones. The other commonly adopted isochrones are those of Ventura et al. (1998) and Y<sup>2</sup>. While the Y<sup>2</sup> models unfortunately do not include the red clump stars, we find that both of these models predict nearly equivalent main sequences, turnoffs, and red giant branches at our range of parameters. We have also compared these isochrones to the most up to date (version 1.2S) PARSEC isochrones (Bressan et al. 2012) from the Padova group. Here, some minor differences are noted in the lowest-mass main sequence stars and the shape of the turnoff, and with respect to Ventura et al. (1998) the red clump stars have subtle differences, but we find these differences do not significantly affect their relative isochrone fits of NGC 2099. These three isochrones find consistent ages of 520 Myr (using those from Ventura et al. 1998 and Y<sup>2</sup>) and 540 Myr (using those from Bressan et al. 2012). We consider these three as our second group of isochrones.

Direct comparison of these two different isochrone groups find that there are significant systematic differences between their evolutionary timescales. At ages appropriate for NGC 2099, the earlier Padova models estimate ages  $\sim 80$  to 100 Myr younger than those of Ventura et al. (1998), Y<sup>2</sup>, and Bressan et al. (2012). Because these up to date Bressan et al. (2012) models have superseded the older Padova isochrones, we take this second isochrone group to provide the better representation of cluster age. This systematic age difference can explain the majority of why studies using the isochrones of either Bertelli et al. (1994), Girardi et al. (2000), or Pietrinferni et al. (2004) consistently found significantly younger ( $\Delta \sim 100$  Myr) ages than K01.

The extremely young age (320 Myr) found in Salaris et al. (2009) and the significantly older age (650 Myr) found in Kalirai et al (2005) still require further explanation. These ages are the result of the adopted metallicity in these two studies. The Salaris et al. (2009) isochrones adopted relatively metal-rich isochrones at  $[\text{Fe}/\text{H}]=0.09 \pm 0.07$ . This higher metallicity primarily shifts the cluster redward in B-V by  $\sim 0.03$ , and this in combination with their large reddening ( $E(B-V)=0.3$ ) required that they adopt a significant distance modulus to provide an appropriate fit to the main sequence. Hence, an isochrone of an additional  $\sim 100$  Myr younger was necessary to match the now relatively quite bright and blue turnoff. In contrast to this, the previous published work in K05 adopted a metal-poor ( $Z=0.011$ ) isochrone, and this change adjusted their original age (520 Myr; K01) upward to (650 Myr). Lastly, in regards to the effects of metallicity, we should comment on why this did not significantly affect the age found by Nilakshi & Sagar et al. (2002). In their case the adopted high reddening counteracted the blue shifting effect of their low metallicity isochrone, giving both an age and distance modulus consistent with the solar metallicity studies. Lastly, as we have discussed, the most recent spectroscopic analyses of NGC 2099 find both  $Z=0.011$  and  $[\text{Fe}/\text{H}]=0.09$  to likely be too extreme, and with our adoption of solar metallicity we continue with the original K01 age of 520 Myr.

## REFERENCES

- Agertz, O., & Kravtsov, A. V. 2014, arXiv:1404.2613  
 An, D., Terndrup, D. M., Pinsonneault, M. H., et al. 2007, ApJ, 655, 233  
 Bergeron, P., Saffer, R. A., & Liebert, J. 1992, ApJ, 394, 228  
 Bergeron, P., Wesemael, F., Dufour, P., et al. 2011, ApJ, 737, 28  
 Bertelli, G., Bressan, A., Chiosi, C., Fagotto, F., & Nasi, E. 1994, A&A, 106, 275  
 Bressan, A., Marigo, P., Girardi, L., et al. 2012, MNRAS, 427, 127  
 Carrera, R., & Pancino, E. 2011, A&A, 535, A30  
 Catalán, S., Isern, J., García-Berro, E., & Ribas, I. 2008, MNRAS, 387, 1693  
 Claver, C. F., Liebert, J., Bergeron, P., & Koester, D. 2001, ApJ, 563, 987  
 Dobbie, P. D., Pinfield, D. J., Napiwotzki, R., et al. 2004, MNRAS, 355, L39

TABLE 3 - Cluster Parameters From Previous Studies

Study	(m-M) <sub>V</sub>	E(B-V)	Metallicity	Age (Myr)	Notes
Mermilliod et al. (1996)	11.50	0.29	Z=0.02	450	Bertelli et al. (1994)
Twarog et al. (1997)	11.55	0.27	[Fe/H]=0.09±0.07	-	DDO Photometric [Fe/H]
Kalirai et al. (2001)	11.55±0.13	0.21±0.03	Z=0.02	520	Ventura et al. (1998)
Kiss et al. (2001)	11.48±0.13	0.29±0.03	Z=0.02	450	Bertelli et al. (1994)
Nilakshi & Sagar (2002)	11.6±0.15	0.30±0.04	Z=0.008	400	Girardi et al. (2000)
Sarajedini et al. (2004)	11.57±0.16	0.27±0.03	[Fe/H]=0.09±0.07	-	E(B-V) and [Fe/H] are from Twarog et al. (1997)
Kalirai et al. (2005)	11.50	0.23±0.01	Z=0.011±0.001	650	Ventura et al. (1998)
Kang et al. (2007)	11.4	0.21	Z=0.019	450	Girardi et al. (2000)
Hartman et al. (2008)	11.57±0.13	0.227±0.038	[Fe/H]=0.045±0.044	485±28	An et al. (2007)
Salaris et al. (2009)	12.00±0.12	0.3	[Fe/H]=0.09±0.15	320±30	Pietrinferni et al. (2004)
	11.40±0.12	0.23	Z=0.011±0.001	550±50	E(B-V) and [Fe/H] are from K05.
Pancino et al. (2010)	11.53±0.19	0.27±0.04	[Fe/H]=0.01±0.05	410±155	Are literature averages other than [Fe/H].

- Dobbie, P. D., Napiwotzki, R., Burleigh, M. R., et al. 2006, MNRAS, 369, 383
- Dobbie, P. D., Napiwotzki, R., Burleigh, M. R., et al. 2009, MNRAS, 395, 2248
- Dobbie, P. D., & Baxter, R. 2010, American Institute of Physics Conference Series, 1273, 31
- Dobbie, P. D., Day-Jones, A., Williams, K. A., et al. 2012, MNRAS, 423, 2815
- Fernie, J. D. 1963, AJ, 68, 780
- Ferrario, L., Wickramasinghe, D., Liebert, J., & Williams, K. A. 2005, MNRAS, 361, 1131
- Fontaine, G., Brassard, P., & Bergeron, P. 2001, PASP, 113, 409
- Fusi-Peccii, F., & Renzini, A. 1976, A&A, 46, 447
- Girardi, L., Bressan, A., Bertelli, G., & Chiosi, C. 2000, A&A, 141, 371
- Greggio, L. 2010, MNRAS, 406, 22
- Gratton, R., Bragaglia, A., Carretta, E., & Tosi, M. 2006, ApJ, 642, 462
- Hartman, J. D., Gaudi, B. S., Holman, M. J., et al. 2008, ApJ, 675, 1254
- Holberg, J. B., & Bergeron, P. 2006, AJ, 132, 1221
- Hurley, J. R., Pols, O. R., & Tout, C. A. 2000, MNRAS, 315, 543
- Jeffries, R. D. 1997, MNRAS, 288, 585
- Kalirai, J. S., Ventura, P., Richer, H. B., et al. 2001, AJ, 122, 3239
- Kalirai, J. S., Richer, H. B., Reitzel, D., et al. 2005, ApJ, 618, L123
- Kalirai, J. S., Bergeron, P., Hansen, B. M. S., et al. 2007, ApJ, 671, 748
- Kalirai, J. S., Saul Davis, D., Richer, H. B., et al. 2009, ApJ, 705, 408
- Kalirai, J. S., Hansen, B. M. S., Kelson, D. D., et al. 2008, ApJ, 676, 594
- Kalirai, J. S. 2013, MmSAI, 84, 58
- Kalirai, J. S., Marigo, P., & Tremblay, P.-E. 2014, ApJ, 782, 17
- Kang, Y. B., Kim, S.-L., Rey, S.-C., et al. 2007, PASP, 119, 239
- Kiss, L. L., Szabó, G. M., Sziládi, K., et al. 2001, A&A, 376, 561
- Kleinman, S. J., Kepler, S. O., Koester, D., et al. 2013, ApJS, 204, 5
- Koester, D., & Reimers, D. 1981, A&A, 99, L8
- Koester, D., & Reimers, D. 1985, A&A, 153, 260
- Koester, D., & Reimers, D. 1993, A&A, 275, 479
- Kowalski, P. M., & Saumon, D. 2006, ApJ, 651, L137
- Liebert, J., Young, P. A., Arnett, D., Holberg, J. B., & Williams, K. A. 2005, ApJ, 630, L69
- Liebert, J., Bergeron, P., & Holberg, J. B. 2005, ApJS, 156, 47
- Marigo, P., & Girardi, L. 2007, A&A, 469, 239
- Meng, X., Chen, X., & Han, Z. 2008, A&A, 487, 625
- Mermilliod, J.-C., Huestamendia, G., del Rio, G., & Mayor, M. 1996, A&A, 307, 80
- Nilakshi, & Sagar, R. 2002, A&A, 381, 65
- Oke, J. B., Cohen, J. G., Carr, M., et al. 1995, PASP, 107, 375
- Pancino, E., Carrera, R., Rossetti, E., & Gallart, C. 2010, A&A, 511, A56
- Pietrinferni, A., Cassisi, S., Salaris, M., & Castelli, F. 2004, ApJ, 612, 168
- Press, W. H., Flannery, B. P., & Teukolsky, S. A. 1986, Cambridge: University Press, 1986,
- Pritchett, C. J., Howell, D. A., & Sullivan, M. 2008, ApJ, 683, L25
- Reimers, D., & Koester, D. 1982, A&A, 116, 341
- Reimers, D., & Koester, D. 1989, A&A, 218, 118
- Reimers, D., & Koester, D. 1994, A&A, 285, 451
- Rubin, K. H. R., Williams, K. A., Bolte, M., & Koester, D. 2008, AJ, 135, 2163
- Salaris, M., Serenelli, A., Weiss, A., & Miller Bertolami, M. 2009, ApJ, 692, 1013
- Sarajedini, A., Brandt, K., Grocholski, A. J., & Tiede, G. P. 2004, AJ, 127, 991
- Tremblay, P.-E., & Bergeron, P. 2008, ApJ, 672, 1144
- Tremblay, P.-E., Bergeron, P., & Gianninas, A. 2011, ApJ, 730, 128
- Twarog, B. A., Ashman, K. M., & Anthony-Twarog, B. J. 1997, AJ, 114, 2556
- Ventura, P., Zeppieri, A., Mazzitelli, I., & D'Antona, F. 1998, A&A, 334, 953
- Weidemann, V. 1977, A&A, 59, 411
- Weidemann, V., & Koester, D. 1983, A&A, 121, 77
- Weidemann, V. 1987, A&A, 188, 74
- Weidemann, V. 2000, A&A, 363, 647
- Williams, K. A., Bolte, M., & Koester, D. 2004, ApJ, 615, L49
- Williams, K. A., & Bolte, M. 2007, AJ, 133, 1490
- Williams, K. A., Bolte, M., & Koester, D. 2009, ApJ, 693, 355
- Yi, S., Demarque, P., Kim, Y.-C., et al. 2001, ApJ, 136, 417